Onset of convection in binary gas mixtures: Role of the Dufour effect

W. Hort
Institut für Theoretische Physik, Universität des Saarlandes, D-6600 Saarbrücken, Federal Republic of Germany

S. J. Linz
Institut für Theoretische Physik, Universität des Saarlandes, D-6600 Saarbrücken, Federal Republic of Germany and Department of Engineering Sciences and Applied Mathematics, Northwestern University, Evanston, Illinois 60208

M. Lücke
Institut für Theoretische Physik, Universität des Saarlandes, D-6600 Saarbrücken, Federal Republic of Germany

(Received 12 August 1991)

The stability behavior of the conductive state of binary gas mixtures in the Rayleigh-Bénard setup is significantly altered in comparison to binary liquid mixtures due to their different thermodynamic and transport properties. In particular, the Dufour effect influences dramatically the topology and the existence ranges of the oscillatory and stationary instabilities for Dufour and Lewis numbers that are typical in gas mixtures. We present a detailed investigation of the changes of the stability properties for several types of boundary conditions including the realistic no-slip, impermeable ones.

PACS number(s): 47.20.−k, 47.10.+g, 47.25.−c, 51.30.+i

I. INTRODUCTION

During the past few years the investigation of convection in binary fluid layers driven by an external temperature gradient has evolved to one of the most intensively studied branches of modern hydrodynamics [1–34]. But up to now most work done in this field has been concerned with binary *liquid* mixtures, perhaps since the fluids used most often in experiments are ethanol-water [2–10] and ^{3}He-^{4}He mixtures [11–13].

Convection in binary fluid mixtures is governed by the time evolution of velocity, temperature, and concentration fields [35,36]. These fields are coupled via buoyancy, convective transport, and diffusive heat and concentration currents. For example, temperature fluctuations are driven in general by heat as well as by concentration currents. In liquid mixtures the contribution from the concentration current to the driving of temperature fluctuations is small in comparison to the heat current and can be neglected in that case.

Recently the drastic influence of concentration currents on temperature fluctuations in gas mixtures was recognized in a system [31] where instead of an external temperature gradient an external concentration gradient is applied. After that we have shown [32,33] that also binary gas mixtures in the Rayleigh-Bénard setup should display convection properties that differ significantly from those in liquid mixtures. These changes arise from the different physical properties of gases and liquids, i.e., their different transport and thermodynamical coefficients. Since the concentration diffusion constant D (the thermal diffusivity κ) of gas mixtures is typically 10^4 times larger (10^2 times larger) than in liquids the Lewis number $L=D/\kappa$ of gas mixtures is about 10^2 times larger than the corresponding one in liquid mixtures. Thus in gases the Lewis number is no longer a small quantity like in liquids where $L\simeq 10^{-2}$, but of the order 1. Even more important are the changes in the Dufour effect: The coupling strength of the diffusive concentration current into the temperature field equation measured by the product of the Lewis number L (a transport quantity) and the Dufour number Q (a thermodynamic quantity explained in Sec. II B) is about 10^4 times larger in gases than in liquids. Thus the Dufour effect can in general no longer be ignored in gases. Earlier work [15–17] done for idealized free-slip, permeable (FSP) boundary conditions on the influence of the Dufour effect was partly concerned with liquid mixtures and there the negligibility of the Dufour terms was shown. Recently Stein [37] has presented results for realistic no slip, impermeable (NSI) boundary conditions, which were obtained by a sine series expansion.

In Ref. [32] we have reported some changes of the stability properties of the conductive state in gases for FSP boundary conditions and Dufour and Lewis numbers that we estimated to be realizable in gas mixtures that were likely candidates for experiments. For FSP conditions the linear stability analysis can be done exactly in full analytical detail in the presence of the Dufour effect. Figure 1 summarizes for the FSP case and a Lewis number $L=\frac{1}{2}$ the characteristic changes with increasing the Dufour number Q from zero up to a value of $Q=12$. The solid (dotted) lines in Fig. 1 denote the stationary (oscillatory) stability threshold of the conductive state as a function of the separation ratio ψ [18] which is defined in Sec. II B. For $Q=0$ (no Dufour coupling) there are no

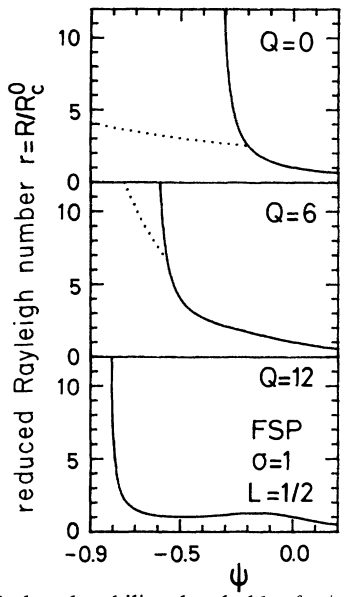

FIG. 1. Reduced stability thresholds $r^c_{\rm stat}$ (solid lines) for stationary and $r^c_{\rm osc}$ (dots) for the oscillatory onset of convection vs. separation ratio ψ for different Dufour numbers Q. Horizontal boundaries are FSP (cf. Sec. III A) with $R_c^0=(27/4)\pi^4$. The Lewis number $L=\frac{1}{2}$ and the Prandtl number $\sigma=1$ are typical for gas mixtures.

topological changes of the stability diagram in comparison to liquid mixtures with small L. Only the codimension-2 (CT) point [18] is shifted to more negative ψ values due to the higher Lewis number. Increasing the Dufour coupling to a value of $Q=6$ leads mainly to a wandering of the CT point to more negative ψ and to a strong stabilization of the conductive state in the range where an oscillatory instability exists. Further increasing to $Q=12$ shows that then also the stationary instability is influenced significantly by the Dufour effect: for not too large negative ψ there is a destabilization with a minimum in $r^c_{\rm stat}$ at $\psi=-0.5$. On the other hand, the oscillatory instability line is shifted to much higher Rayleigh numbers and its existence range is strongly diminished so that it can no longer be seen in Fig. 1.

In this paper we want to give a fuller account of the linear stability properties for different boundary conditions. Our paper is organized as follows. In Sec. II we review the basic equations governing convection in binary mixtures in the Rayleigh-Bénard setup. Section III presents analytical calculations of the stability properties for idealized free-slip permeable and impermeable boundary conditions. In Sec. IV the full numerical stability analysis for realistic no-slip boundary conditions is discussed. There we also discuss the stability behavior of the conductive state for heating the fluid layer from above. Section V summarizes our results. In the Appendix we give an ideal-gas approximation to calculate the Dufour number and estimate when the compressibility of the gas mixture influences the stability behavior significantly.

II. SYSTEM

In part A of this section we review the basic equations [35,36,38] describing convection in binary mixtures. In part B we present for the Rayleigh-Bénard setup our scaled Oberbeck-Boussinesq equations and in part C the linearized equations. Finally we estimate in part D the magnitude of the physical parameters, in particular the Dufour number, in gas mixtures.

A. Governing equations

The hydrodynamic equations for the fields of velocity $\mathbf{u}$, temperature T, concentration C, and mass density ρ describing convection in binary fluid mixtures are [35,36,38]

$$\rho(\partial_t+\mathbf{u}\cdot\nabla)\mathbf{u}=-\nabla p+\rho\mathbf{g}+\nabla\cdot\overleftrightarrow{\sigma}' , \tag{2.1a}$$

$$c_p\rho(\partial_t+\mathbf{u}\cdot\nabla)T=\epsilon+[\mu-T(\partial\mu/\partial T)_{C,p}]\nabla\cdot\mathbf{J}_c-\nabla\cdot\mathbf{J}_e , \tag{2.1b}$$

$$\rho(\partial_t+\mathbf{u}\cdot\nabla)C=-\nabla\cdot\mathbf{J}_c , \tag{2.1c}$$

$$\partial_t\rho+\nabla\cdot(\rho\mathbf{u})=0 . \tag{2.1d}$$

Here p is the pressure, ϵ the energy dissipation rate, $\mathbf{g}$ the gravitational acceleration, $\overleftrightarrow{\sigma}'$ the viscosity stress tensor [35], c_p the specific heat at constant T, p, and C, and μ the chemical potential [35] of the binary mixture. The diffusive currents of concentration and energy $\mathbf{J}_c$ and $\mathbf{J}_e$ are obtained from Onsager's theory of linear nonequilibrium thermodynamics. There one can show that the entropy production rate dS/dt is given by the volume integral

$$\frac{dS}{dt}=\int dV\left[\sum_{i=1}^{2}\mathbf{J}_i\cdot\mathbf{F}_i+\frac{\epsilon}{T}\right] , \tag{2.2a}$$

where $\mathbf{J}_i$ are the above two diffusive currents and $\mathbf{F}_i$ the associated generalized forces driving the currents. They couple via linear Onsager relations:

$$\mathbf{J}_i=\sum_{k=1}^{2}L_{ik}\mathbf{F}_k . \tag{2.2b}$$

The Onsager coefficients L_{ik} are for time-reversal invariant forces $\mathbf{F}_i$ symmetric, $L_{ik}=L_{ki}$. Thermodynamic considerations based on entropy growth processes show that the generalized forces for binary mixtures are

$$\mathbf{F}_e=\nabla\left[\frac{1}{T}\right] \text{ and } \mathbf{F}_c=-\nabla\left[\frac{\mu}{T}\right] . \tag{2.3}$$

With the local chemical potential $\mu(T,p,C)$ depending on temperature, pressure, and concentration, its gradient is given by

$$\nabla\mu=\left[\frac{\partial\mu}{\partial T}\right]_{C,p}\nabla T+\left[\frac{\partial\mu}{\partial C}\right]_{T,p}\nabla C+\left[\frac{\partial\mu}{\partial p}\right]_{C,T}\nabla p .$$

Thus the currents can be written as

$$\mathbf{J}_e=\left[k_T\left[\frac{\partial\mu}{\partial C}\right]_{T,p}+\mu-T\left[\frac{\partial\mu}{\partial T}\right]_{C,p}\right]\mathbf{J}_c-\lambda\nabla T , \tag{2.4a}$$

$$\mathbf{J}_c=-\rho D[\nabla C+k_T(\nabla T/T)+k_p(\nabla p/p)] . \tag{2.4b}$$

The coefficients k_T, λ, D, and k_p are the

thermodiffusivity, the heat conductivity, the concentration diffusion coefficient, and the barodiffusion coefficient. They are combinations of Onsager coefficients and derivatives of the chemical potential and are experimentally accessible [35].

The fact that a temperature gradient drives according to (2.4b) a concentration current is the Soret effect. The concentration current $\mathbf{J}_c$ drives according to (2.1b) temperature fluctuations directly and indirectly via $\mathbf{J}_e$ (2.4a). These couplings are the Dufour effect. The sum of these contributions to the right-hand side (rhs) of (2.1b) yields the term $k_T(\partial\mu/\partial T)_{C,p}\nabla\cdot\mathbf{J}_c$. Its size in liquid mixtures is small compared to the Fourier contribution $\lambda\nabla^2 T$, but not in gases.

B. Oberbeck-Boussinesq approximation

The system we discuss in the following is a horizontal binary fluid layer of vertical extension d. Perfectly heat conducting boundaries impose a temperature difference ΔT between the bottom $T_0+\Delta T$ at $z=-d/2$ and the top T_0 at $z=d/2$. We restrict ourselves to a situation where the fields T, C, and p in the fluid layer deviate only slightly from their reference values, say, at the top plate. These reference values are marked by an index 0 in the following. Then the Oberbeck-Boussinesq approximation may be used where the spatiotemporal variation of all transport and thermodynamic coefficients is neglected by evaluating them for the reference values. Furthermore, the deviation of the total mass density from the reference state may be ignored except in the vertical buoyancy force density $\rho\mathbf{g}$. There, for small deviations of T, C, and p one can expand the equation of state

$$\rho=\rho_0[1-\alpha(T-T_0)-\beta(C-C_0)+\chi(p-p_0)] . \tag{2.5}$$

Here the thermal and solutal expansion coefficients are defined by $\alpha=-(1/\rho_0)(\partial\rho/\partial T)^0_{C,p}$ and $\beta=-(1/\rho_0)(\partial\rho/\partial C)^0_{T,p}$, respectively. The compressibility coefficient $\chi=(1/\rho_0)(\partial\rho/\partial p)^0_{C,T}$ is small in liquid as well as in gas mixtures (cf. Appendix) and will be ignored in the following. Finally the energy dissipation ϵ can be ignored.

We reduce lengths by d, times by d^2/κ, temperatures by $\kappa\nu/\alpha g d^3$, concentration by $\kappa\nu/\beta g d^3$, and p/ρ_0 by κ^2/d^2 where ν is the kinematic viscosity. Then the field equations (2.1) read in the Oberbeck-Boussinesq approximation

$$(\partial_t+\mathbf{u}\cdot\nabla)\mathbf{u}=-\nabla(p+\hat{g}z)+\mathbf{e}_z\sigma(T-T_0+C-C_0)+\sigma\nabla^2\mathbf{u} , \tag{2.6a}$$

$$(\partial_t+\mathbf{u}\cdot\nabla)T=(1+QL\psi^2)\nabla^2 T-QL\psi\nabla^2 C , \tag{2.6b}$$

$$(\partial_t+\mathbf{u}\cdot\nabla)C=L\nabla^2(C-\psi T) , \tag{2.6c}$$

$$\nabla\cdot\mathbf{u}=0 . \tag{2.6d}$$

Here we have introduced the Prandtl number $\sigma=\nu/\kappa$, the Lewis number $L=D/\kappa$, and the dimensionless gravitational constant $\hat{g}=gd^3/\kappa^2$. The separation ratio

$$\psi=-\frac{\beta}{\alpha}\frac{k_T}{T_0} \tag{2.7}$$

can be positive or negative while the Dufour number

$$Q=\frac{T_0\alpha^2}{c_p\beta^2}\left[\frac{\partial\mu}{\partial C}\right]^0_{T,p} \tag{2.8}$$

is always positive [35]. Since in gas mixtures the barodiffusion contribution is only of importance for separation ratios of the order 10^{-6} we will ignore it in the following.

Note that the Dufour terms enter into the temperature field equation (2.6b) via a "diagonal" coupling to $\nabla^2 T$ with strength $QL\psi^2$ and via an "offdiagonal" coupling to $\nabla^2 C$ with strength $-QL\psi$.

C. Linearization around the conductive state

In the motionless conductive state (marked in the following by the index "cond") $\mathbf{u}$ is zero. The temperature and concentration fields are stationary, horizontally homogeneous, and depend on z only linearly. Since the boundaries at $z=\pm\frac{1}{2}$ are impermeable the conductive concentration current $\mathbf{J}_c^{\rm cond}$ has to be zero there. The structure of the conductive fields then enforces that the current vanishes globally in the conductive state

$$\mathbf{J}_c^{\rm cond}=-L\nabla(C_{\rm cond}-\psi T_{\rm cond})=0 . \tag{2.9}$$

So the vertical concentration stratification is tied to that of the temperature via the Soret effect. The conductive profiles

$$T_{\rm cond}(z)-T_0=R(\tfrac{1}{2}-z) , \tag{2.10a}$$

$$C_{\rm cond}(z)-C_m=-R\psi z \tag{2.10b}$$

are not influenced by the Dufour effect. Here T_0 is the reduced temperature at the top boundary and the Rayleigh number

$$R=\frac{\alpha g d^3}{\kappa\nu}\Delta T \tag{2.10c}$$

is the reduced temperature difference across the fluid layer. C_m is the reduced mean concentration and $C_0=C_m-R\psi/2$ is the concentration at the top. The Soret induced concentration difference between top and bottom, $\Delta C=-R\psi$, and C_0 depend on the product $R\psi$.

To discuss the stability of the conductive state we write down the linearized equations for the deviations from the conductive state

$$(\partial_t-\sigma\nabla^2)\nabla^2 w=\sigma[\partial_x^2+\partial_y^2](\theta+c) , \tag{2.11a}$$

$$\partial_t\theta=Rw+(1+LQ\psi^2)\nabla^2\theta-LQ\psi\nabla^2 c , \tag{2.11b}$$

$$\partial_t c=R\psi w+L\nabla^2(c-\psi\theta) , \tag{2.11c}$$

where $\theta=T-T_{\rm cond}$, $c=C-C_{\rm cond}$, and w is the vertical component of the velocity $\mathbf{u}$. Here we have taken twice the curl of (2.6a) using (2.6d).

D. The Dufour number

To get a feeling for the magnitude of the Dufour number Q we estimate its value for typical liquid and gas mixtures. Estimates [22] for ethanol-water mixtures at room temperature show that $\alpha \simeq 3\times 10^{-4}/K$, $\beta \simeq 0.2$, $c_p \simeq 4$ W sec/(g K), and $(\partial\mu/\partial C)_{T,p} \simeq 3.2\times 10^9$ cm^2/sec^2 leading to a Dufour number $Q \simeq 0.1$. In contrast to that for gas mixtures $\alpha \simeq 1/(273\ \text{K})$, $\beta \simeq 0.2$, $c_p \simeq 1$ W sec/(g K) and $(\partial\mu/\partial C)_{T,p} \simeq 10^9$ cm^2/sec^2 are typical leading to a Dufour number $Q \simeq 10$. Thus the Dufour number in gas mixtures is about 10^2 times larger than in liquid mixtures. This is basically caused by the fact that the thermal expansion coefficient α entering quadratically into Q is ten times larger in gas mixtures than in liquids. Since the diffusion coefficient D is about 10^{-5} cm^2/sec in liquids versus about 10^{-1} cm^2/sec in gases and the thermal diffusivity κ is about 10^{-3} cm^2/sec in liquids in comparison to about 10^{-1} cm^2/sec in gases, the Lewis number in gases is 10^2 times larger in gas mixtures and of the order 1 and thus no longer a small quantity.

Since the Dufour contributions in the temperature field equation (2.11b) are proportional to $QL\psi$ the Dufour effect is for the same fixed ψ about 10^4 times larger in gas mixtures than in liquid mixtures and no longer negligible if the absolute value of ψ is not too small.

III. ANALYTIC STABILITY ANALYSES

Here we present two analytic approaches to study the changes due to the Dufour effect using two different idealized boundary conditions on the convective disturbances. The purpose of this section is twofold. On one hand we show that the main changes can be understood by these idealizations; on the other hand one can identify by comparing with the full numerical treatment for realistic boundary conditions in Sec. IV which boundary conditions are responsible for additional qualitative changes.

A. FSP boundary conditions

Free-slip permeable boundary conditions on the deviations from the conductive state are the most idealized ones, but on the other hand the easiest ones to calculate. They are defined by

$$w = \partial_z^2 w = \theta = c = 0 \quad \text{at } z = \pm\tfrac{1}{2} . \tag{3.1}$$

With $c=0$ at the boundaries there can be vertical concentration gradients and with it vertical concentration currents through the top and bottom boundaries—hence the name permeable. The stability analysis can be carried out in full exact analytical detail. The solution for disturbances, e.g., with lateral wave numbers $k_x = k$, $k_y = 0$ is

$$w(x,z,t) = [\bar{w}(t)e^{ikx} + \text{c.c.}]\sqrt{2}\sin\pi(z-\tfrac{1}{2}) , \tag{3.2a}$$

$$\theta(x,z,t) = [\bar{\theta}(t)e^{ikx} + \text{c.c.}]\sqrt{2}\sin\pi(z-\tfrac{1}{2}) , \tag{3.2b}$$

$$c(x,z,t) = [\bar{c}(t)e^{ikx} + \text{c.c.}]\sqrt{2}\sin\pi(z-\tfrac{1}{2}) . \tag{3.2c}$$

It fulfills the boundary conditions (3.1) as well as the linearized equations (2.11). Insertion of (3.2) into (2.11) and performing standard stability analysis leads to the following stability thresholds.

(i) Stationary instability. The conductive state loses its stability against monotonous growth of the convective roll pattern (3.2) at the reduced threshold

$$r_{\text{stat}}(\hat{k}) = (\hat{q}^6/\hat{k}^2) r^c_{\text{stat}} , \tag{3.3a}$$

$$r^c_{\text{stat}} = \frac{1}{(1+\psi)(1+Q\psi^2)+\psi/L} . \tag{3.3b}$$

(ii) Oscillatory instability. There is a Hopf bifurcation threshold with oscillatory growth of the convective disturbances (3.2) at

$$r_{\text{osc}}(\hat{k}) = (\hat{q}^6/\hat{k}^2) r^c_{\text{osc}} , \tag{3.4a}$$

$$r^c_{\text{osc}} = \frac{1}{\sigma}\frac{L(1+Q\psi^2)[\sigma(\sigma+2)+L+L\sigma(1+Q\psi^2)]+\sigma^2+\sigma+L}{1+(1+\psi)\sigma} \tag{3.4b}$$

with frequency

$$\omega(\hat{k}) = \hat{q}^2\omega_c \tag{3.5a}$$

as long as the square of the Hopf frequency

$$\omega_c^2 = -\tfrac{9}{4}\pi^4\frac{L[1+\sigma(1+Q\psi^2)][\psi+L(1+\psi)(1+Q\psi^2)]+\sigma\psi[1+LQ\psi(1+\psi)]}{1+(1+\psi)\sigma} \tag{3.5b}$$

is non-negative. Here we have reduced by critical quantities in the pure fluid $\psi=0$ with FS boundaries

$$r = R/R_c^0, \quad R_c^0 = 27\pi^4/4 , \tag{3.6a}$$

$$\hat{k} = k/k_c^0, \quad k_c^0 = \pi/\sqrt{2}, \quad \hat{q}^2 = (k^2+\pi^2)/[(k_c^0)^2+\pi^2] . \tag{3.6b}$$

For the oscillatory as well as the stationary thresholds in mixtures the critical wave numbers are independent of L, ψ, Q, and σ and coincide for FSP boundaries with the critical wave number in the pure fluid $k^c_{\text{osc}} = k^c_{\text{stat}} = k_c^0 = \pi/\sqrt{2}$. Setting $Q=0$ the results [1,18,36] without the Dufour effect are obtained. The critical values r^c_{stat} and r^c_{osc} are shown in Fig. 1 for a gas mixture of $\sigma=1$, $L=\frac{1}{2}$, and three different Dufour numbers as a function of ψ. When the system is heated from below a stationary instability exists whenever $\psi > \psi^\infty_{\text{stat}}$ with $\psi^\infty_{\text{stat}}$

given by the zero of the denominator of (3.3b). A large-Q expansion shows [32] that $r^c_{\rm stat}$ diverges at $\psi^\infty_{\rm stat}(Q\gg 1)=-1+(LQ)^{-1}+O(Q)^{-2}$. Note that $\psi^\infty_{\rm stat}>-1$ for finite Dufour numbers. From (3.3b) one immediately reads off that the incorporation of the Dufour effect $Q\neq 0$ diminishes the stationary stability threshold $r^c_{\rm stat}$ for fixed ψ and L in comparison to the case $Q=0$:

$$r^c_{\rm stat}(Q>0)<r^c_{\rm stat}(Q=0)\ . \tag{3.7a}$$

While $r^c_{\rm stat}(Q=0)$ decreases monotonically from $+\infty$ at $\psi^\infty_{\rm stat}(Q=0)=-L/(L+1)$ to zero at $\psi\to\infty$ the behavior is different if $Q>3(1+1/L)$. Then $r^c_{\rm stat}$ develops a maximum and a minimum at

$$\psi_\pm=-\frac{1}{3}\left[1\pm\left[1-\frac{3(1+L)}{QL}\right]^{1/2}\right]$$

as shown in Fig. 1 for $L=\frac{1}{2}$ and $Q=12$. With increasing Q the maximum (minimum) approaches $\psi=0$ ($\psi=-\frac{2}{3}$) and leads to a strong destabilization of the conductive state.

When the system is heated from above, i.e., $r<0$, one has to distinguish between the case $\psi<-1$ and the case $-1<\psi<\psi^\infty_{\rm stat}$. From Eq. (3.3) one reads off that in the former (latter) case the absolute value of $r^c_{\rm stat}$ is diminished (enhanced) by the Dufour effect, implying a destabilization for $\psi<-1$ (stabilization for $-1<\psi<\psi^\infty_{\rm stat}$). For $\psi=-1$ the Dufour effect has no influence on the stationary stability threshold, since there $r^c_{\rm stat}(\psi=-1)=-L$.

Let us now turn to the oscillatory instability. For FSP boundary conditions the lower bound of existence of oscillatory instabilities where $r^c_{\rm osc}$ and ω_c diverges is not changed by the Dufour effect and is given by $\psi^\infty_{\rm osc}=-(1+1/\sigma)$. In the case $Q=0$ there is a single CT point [18] at $\psi_{\rm CT}=-(1+\sigma)/(1+\sigma+L^{-1}+\sigma/L+\sigma/L^2)$ at which the frequency ω_c vanishes and simultaneously $r^c_{\rm osc}=r^c_{\rm stat}$. For finite Q, however, $\psi_{\rm CT}$ is determined by the zeros of a fifth-order polynomial in ψ. Thus depending on Q more than one CT point can exist, e.g., three, and there can be several ranges where oscillatory instabilities can exist. Moreover one can read off from (3.4) that for any fixed L,ψ

$$r^c_{\rm osc}(Q>0)>r^c_{\rm osc}(Q=0)\ . \tag{3.7b}$$

Thus the conductive state is always stabilized against oscillatory convection by the Dufour effect, the stronger the larger Q. In the limit $Q\to\infty$ $r^c_{\rm osc}$ diverges for all ψ with a positive ω_c^2. For large Q one can show that there is a single CT point at $\psi_{\rm CT}=-1+(LQ)^{-1}+O(Q)^{-2}$ and $r_{\rm CT}=L^2Q^2+O(Q)$. But more importantly, $\psi_{\rm CT}$ is always bigger than $\psi^\infty_{\rm stat}$ since from the large-Q expansion follows [32]

$$\psi_{\rm CT}-\psi^\infty_{\rm stat}=L^{-2}Q^{-3}+O(Q^{-4})\ .$$

Therefore also for large Q there exists always a ψ range where the oscillatory threshold lies below the stationary one. Only in the limit $Q\to\infty$ does this range disappear. A finite Dufour effect leads to a diminishing of the oscillatory range but *not* to a vanishing.

Also for a Lewis number $L=1$ an oscillatory threshold exists in any case whether $Q=0$ or finite. This indicates that the argument [39] that oscillatory convection is basically caused by the difference of thermal and concentration diffusivities is incomplete. Instead it is the Soret induced offdiagonal coupling of the temperature and concentration modes that lead to an oscillatory dynamics.

As we show in Sec. IV the main topological changes of the stability curves induced by the Dufour effect are recovered qualitatively also for realistic no-slip boundary conditions.

B. FSI boundary conditions

With free-slip, impermeable (FSI) boundary conditions for the convective perturbations

$$w=\partial_z^2 w=\theta=\partial_z(c-\psi\theta)=0 \quad \text{at } z=\pm\tfrac{1}{2} \tag{3.8}$$

the vertical concentration current through the boundaries is enforced to vanish. So FSI conditions are more realistic than FSP but still not fully realistic. It was shown earlier [21] that the impermeability has a drastic influence on linear as well as on nonlinear convective properties. Here we present an analytic stability analysis including the Dufour effect that is in contrast to the FSP case only approximate. It is based upon the trial functions [21]

$$w(x,z,t)=[\tilde{w}(t)e^{ikx}+\text{c.c.}]\sqrt{2}\sin\pi(z-\tfrac{1}{2})\ , \tag{3.9a}$$

$$\theta(x,z,t)=[\tilde{\theta}(t)e^{ikx}+\text{c.c.}]\sqrt{2}\sin\pi(z-\tfrac{1}{2})\ , \tag{3.9b}$$

$$\zeta(x,t)=\tilde{\zeta}(t)e^{ikx}+\text{c.c.} \tag{3.9c}$$

which fulfill the boundary conditions, but solve the basic equations only approximately.

In writing down (3.9c) we have introduced the field

$$\zeta=c-\psi\theta\ , \tag{3.10}$$

whose z derivative has to vanish at the impermeable plates. Using (3.10) the linearized field equations (2.11) now read

$$(\partial_t-\sigma\nabla^2)\nabla^2 w=\sigma(\partial_x^2+\partial_y^2)[(1+\psi)\theta+\zeta]\ , \tag{3.11a}$$

$$(\partial_t-\nabla^2)\theta=Rw-LQ\psi\nabla^2\zeta\ , \tag{3.11b}$$

$$[\partial_t-L(1+Q\psi^2)\nabla^2]\zeta=-\psi\nabla^2\theta \tag{3.11c}$$

with the boundary conditions (3.8). Two remarks are in order. First, by introducing the ζ field ψ appears explicitly in the buoyancy in (3.11a). Second, the Dufour effect now enters not only in the θ-field equation via $-LQ\psi\nabla^2\zeta$ but also in the ζ-field equation. There it changes the "diffusion constant" of the ζ field from L for $Q=0$ to $L(1+Q\psi^2)$. Thus large Dufour numbers Q and not too small ψ can significantly enhance this effective Lewis number $L(1+Q\psi^2)$.

For FSI boundary conditions (3.8) the stationary stability threshold evaluated for the perturbation fields (3.9) reads

$$r_{\text{stat}}(\hat{k})=\frac{\hat{q}^6}{\hat{k}^2}\frac{1+Q\psi^2(1-8/\pi^2)}{(1+\psi)\hat{L}(1+Q\psi^2)+8\psi/\pi^2}\hat{L} \ . \quad (3.12)$$

Here r, $\hat{k}$, and $\hat{q}$ are reduced as in (3.6) by the FS critical values of the pure fluid. Furthermore

$$\hat{L}=\frac{\hat{k}^2}{2+\hat{k}^2}L \ . \quad (3.13)$$

The FSI critical wave number of the stationary instability depends, in contrast to the FSP result, on ψ, L, and Q:

$$(\hat{k}^c_{\text{stat}})^2=\frac{(1+\psi)L(1+Q\psi^2)-16\psi/\pi^2}{(1+\psi)L(1+Q\psi^2)+8\psi/\pi^2} \ . \quad (3.14)$$

By setting $Q=0$ we recover the formulas of Ref. [21]. The behavior of the FSI critical stability curve r^c_{stat} is very similar to the FSP case: For $Q=0$ it diverges at $\psi^\infty_{\text{stat}}=-\hat{L}/(\hat{L}+8/\pi^2)$ and decreases monotonically with increasing ψ (Fig. 2; $Q=0$). With increasing Q the divergence shifts to smaller ψ and the curve changes its shape (Fig. 2; $Q=5$). By further increasing Q the stability curve is no longer monotonic. It develops a local maximum and minimum (Fig. 2; $Q=10$). More enlarged Dufour numbers Q lead to an accentuation of this behavior (Fig. 2; $Q=20$). A large-Q expansion shows that the stationary stability curve diverges at

$$\psi^\infty_{\text{stat}}(Q\gg 1)=-1+(8/\pi^2)(\hat{L}Q)^{-1}+O(Q^{-2}) \ , \quad (3.15)$$

differing only slightly from the FSP case. In the $Q\to\infty$ limit r^c_{stat} diverges at $\psi=-1$, is equal to 1 at $\psi=0$, and is $r^c_{\text{stat}}=(1-8/\pi^2)/(1+\psi)$ elsewhere. Thus the Dufour effect leads to a strong downward shift of the stationary threshold r^c_{stat} as with FSP boundary conditions.

Within the FSI approximation information about the ψ dependence of the critical wave numbers can also be obtained. The critical wave number of the stationary instability $\hat{k}^c_{\text{stat}}$ decreases for $Q=0$ monotonically from ∞ at $\psi(Q=0,\ k^c_{\text{stat}}=\infty)=-L/(L+8/\pi^2)$ to zero at $\psi(Q=0,k^c_{\text{stat}}=0)=-L/(L-16/\pi^2)$ (if $L<16/\pi^2$) and remains zero for larger ψ. However, for finite Q the curve $\hat{k}^c_{\text{stat}}$ is no longer monotonically decreasing with increasing ψ. The equation $(\hat{k}^c_{\text{stat}})^2=0$ is a polynomial of order three and has for small Q three real roots. One of these roots lies for all $Q>0$ in the range $\psi<-1$. The other two in the range $\psi>0$ shift together when increasing the Dufour number until they coincide and create a double root. For larger Q then, there remains only the root in the range $\psi<-1$. However, in the positive-ψ range the curve $\hat{k}^c_{\text{stat}}(\psi)$ develops a minimum after the two roots have coalesced. This minimum approaches zero in the limit $Q\to\infty$. For the gas mixture with $L=1$, $\sigma=1$ in Fig. 2 the minimum lies at $\psi\simeq 0.19$ for a Dufour number $Q=20$. If we further increase the Dufour number then the curve $\hat{k}^c_{\text{stat}}(\psi)$ develops for $Q=27$ a saddle at $\psi=-\frac{1}{3}$. Thereafter there appears an additional minimum (maximum), which in the limit $Q\to\infty$ moves towards $\psi=-\frac{1}{2}$ ($\psi=0$). In this limit $\hat{k}^c_{\text{stat}}$ diverges at $\psi=-1$ and is $\hat{k}^c_{\text{stat}}=1$ elsewhere. The large-Q expansion shows that the divergence of $\hat{k}^c_{\text{stat}}$ at

$$\psi(\hat{k}^c_{\text{stat}}\to\infty)=-1+(8/\pi^2)(LQ)^{-1}+O(Q^{-2}) \quad (3.16)$$

lies at smaller values than the divergence of r^c_{stat} since $L>\hat{L}$.

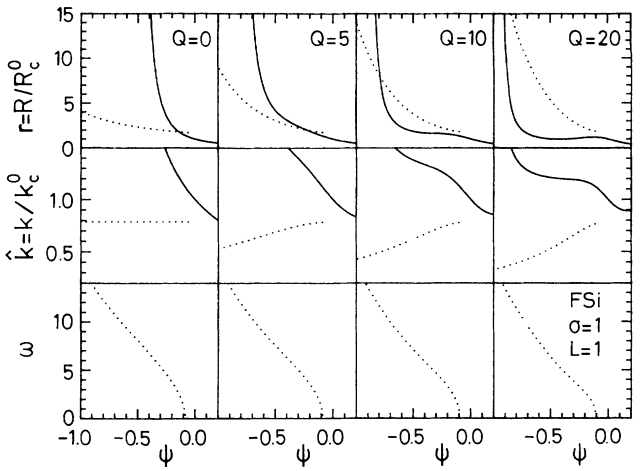

FIG. 2. Stability properties of a gas mixture ($L=1$, $\sigma=1$) vs separation ratio ψ for different Dufour numbers Q. The stationary (solid line) and oscillatory (dotted line) stability thresholds r^c_{stat} and r^c_{osc}, the corresponding reduced critical wave numbers $\hat{k}^c_{\text{stat}}$ and $\hat{k}^c_{\text{osc}}$, and the Hopf frequency ω_c are determined approximately for FSI boundaries (cf. Sec. III B) for which $R^0_c=(\frac{27}{4})\pi^4$ and $k^0_c=\pi/\sqrt{2}$.

In case of the oscillatory instability the conductive state loses its stability at

$$r_{\text{osc}}(\hat{k})=\frac{\hat{q}^6}{\hat{k}^2}\left[\frac{(1+\sigma)[1+\hat{L}(1+Q\psi^2)][1+\hat{L}(1+Q\psi^2)/\sigma]-\hat{L}Q\psi^2(8/\pi^2)[1+\sigma+\hat{L}(1+Q\psi^2)]}{(1+\psi)(1+\sigma)-8\psi/\pi^2}\right] \quad (3.17)$$

as long as the square of the Hopf frequency

$$\frac{\omega^2(\hat{k})\tau^2}{\hat{q}^2}=-[\hat{L}(1+Q\psi^2)]^2-\frac{(8/\pi^2)\psi[1+\hat{L}(1+Q\psi^2)][\sigma+\hat{L}(1+Q\psi^2)]}{(1+\psi)(1+\sigma)-\psi 8/\pi^2}+\frac{\hat{L}Q\psi^2(8/\pi^2)\sigma[(8/\pi^2)\psi+(1+\psi)\hat{L}(1+Q\psi^2)]}{(1+\psi)(1+\sigma)-\psi 8/\pi^2} \quad (3.18)$$

is non-negative. Here $\tau=1/[(k^0_c)^2+\pi^2]$. The critical wave number $\hat{k}^c_{\text{osc}}$ of the oscillatory instability is Q and ψ dependent and can be determined as the real root of

$$0=(\hat{k}^c_{\rm osc})^6\{[1+L(1+Q\psi^2)][1+L(1+Q\psi^2)/\sigma]-LQ\psi^2(8/\pi^2)[1+L(1+Q\psi^2)/(1+\sigma)]\}$$
$$+(\hat{k}^c_{\rm osc})^4\{3+2L(1+Q\psi^2)(1+1/\sigma)+L^2(1+Q\psi^2)^2/\sigma-LQ\psi^2(8/\pi^2)[2+L(1+Q\psi^2)/(1+\sigma)]\}-4\ . \quad (3.19)$$

While Eq. (3.19) is analytically solvable, we have analyzed it numerically by a Newton method. In the limit $Q\to\infty$ the critical wave number $\hat{k}^c_{\rm osc}$ vanishes. A striking difference in comparison with the FSP case and with the FSI case without Dufour effect where $\hat{k}^c_{\rm osc}=1$ is the fact that $\hat{k}^c_{\rm osc}$ decreases with growing Q and decreasing ψ as shown in Fig. 2. This implies large wave-number gaps $\hat{k}^c_{\rm stat}-\hat{k}^c_{\rm osc}$ at those ψ^* where $r^c_{\rm stat}=r^c_{\rm osc}$.

We should like to mention that the degeneracy of the FSP CT point is lifted already for $Q=0$ by impermeable boundaries [21]: the intersection point ψ^* where $r^c_{\rm stat}=r^c_{\rm osc}$ does not coincide with the end point $\psi^{\rm end}_{\rm osc}$ of the oscillatory threshold $r^c_{\rm osc}$ where the Hopf frequency ω_c vanishes. Only by fixing the wave numbers $k_{\rm osc}$ and $k_{\rm stat}$ to be the same, say $k_{\rm CT}$, does one get a true CT point with $r_{\rm stat}(k_{\rm CT})=r_{\rm osc}(k_{\rm CT})$ and $\omega(k_{\rm CT})=0$.

The divergence of the oscillatory stability threshold $r^c_{\rm osc}$ is not affected by the Dufour effect. It remains at $\psi^\infty_{\rm osc}=-(1+\sigma)/[1+\sigma-(8/\pi^2)]$. But in the whole existence range of the oscillatory instability the Dufour effect leads to an enhancement of $r^c_{\rm osc}$ (cf. Fig. 2). While the FSI displacement of the end point $\psi^{\rm end}_{\rm osc}$ with increasing Dufour number is not as large as for FSP boundary conditions, the enlargement of $r^c_{\rm osc}$ and the depression of $r^c_{\rm stat}$ shifts the FSI intersection points ψ^* to much smaller ψ values (Fig. 2).

IV. STABILITY PROPERTIES OF THE SYSTEM WITH NSI BOUNDARY CONDITIONS

No-slip, impermeable boundary conditions

$$w=\partial_z w=\theta=\partial_z(c-\psi\theta)=0 \quad \text{at } z=\pm\tfrac{1}{2} \quad (4.1)$$

are the most realistic ones with respect to the experimental setups of Refs. [1–13]. With this kind of boundary conditions the stability analysis has to be done numerically to get exact solutions. We have determined oscillatory and stationary stability thresholds $r^c_{\rm osc}$, $r^c_{\rm stat}$, the corresponding reduced critical wave numbers $\hat{k}^c_{\rm osc}$, $\hat{k}^c_{\rm stat}$ and the Hopf frequency ω_c for several parameter values by applying a standard shooting method [33]. Within this method Eqs. (3.11) were solved for marginally stable convective perturbations of the conductive state at threshold that have the form

$$f(x,z,t)=\tilde{f}(z)e^{ikx}e^{i\omega t} \quad (4.2)$$

appropriate for straight parallel rolls with axes in the y direction. The NSI critical values have been reduced throughout this paper by the NS critical values of the pure fluid, $R^0_c=1707.762$ and $k^0_c=3.116\,32$, respectively.

Here we present in detail results for Lewis numbers $L=\frac{1}{2}$, $L=1$ and the Prandtl number $\sigma=1$ which is typical for gas mixtures. We discuss heating from below, i.e., $r>0$, as well as heating from above, i.e., $r<0$.

A. Heating from below

In Fig. 3 we show for a gas mixture with $L=\frac{1}{2}$, $\sigma=1$, and Dufour numbers $Q=0,5,10,20$ the critical values as a function of the separation ratio ψ. Without the Dufour effect $Q=0$ the curves show similar behavior as in liquid mixtures [23,24] with a small L. Here, however, as a result of the large Lewis number, the intersection of $r^c_{\rm stat}$ and $r^c_{\rm osc}$ is shifted to a more negative separation ratio $\psi^*\simeq-0.08$ and the wave number gap is larger there, $\Delta\hat{k}_c(\psi^*)\simeq0.2$. Increasing the Dufour number to $Q=5$ again shifts the divergence of $r^c_{\rm stat}$ to a more negative ψ and bends $r^c_{\rm osc}$ upward leading to a destabilization (stabilization) of the conductive state against stationary (oscillatory) perturbations as for the idealized boundary conditions discussed in Sec. III. However for the NSI condition the critical wave number of the oscillatory instability is now no longer a monotonous function of ψ. It decreases for small $|\psi|$, develops a minimum at $\psi\simeq-0.75$, and then increases for more negative ψ. On the other hand, $\hat{k}^c_{\rm stat}$ begins the development that can be seen already in the FSI approximation. By further increasing of the Dufour number to 10 or 20 $r^c_{\rm stat}$ develops a local minimum and maximum. To illustrate this behavior we show in Fig. 4 the stationary stability threshold as a function of ψ for $Q=0,2,4,\ldots,20$. For $Q=12$ the curve has just formed a minimum-maximum pair. For $Q=20$ the minimum (maximum) lies at $\psi_{\rm min}\simeq-0.58(\psi_{\rm max}\simeq-0.12)$.

The bending down of $r^c_{\rm stat}$ and the slight bending up of $r^c_{\rm osc}$ leads to multiple intersections of the two stability

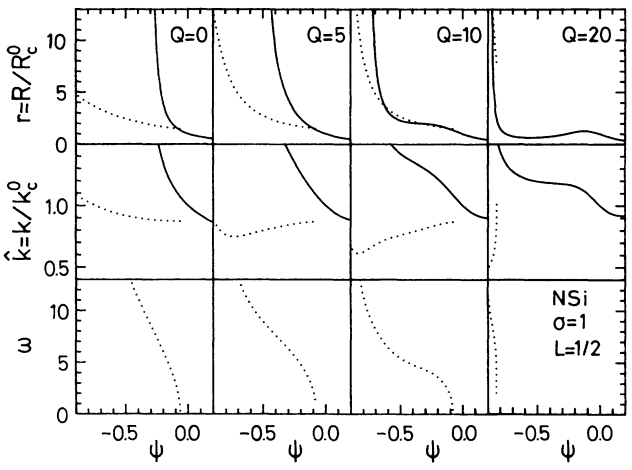

FIG. 3. Exact stability properties of a gas mixture ($L=\frac{1}{2}$, $\sigma=1$) for different Dufour numbers Q. The critical values for the onset of stationary (solid lines) and oscillatory (dots) convection are calculated for realistic NSI boundaries (cf. Sec. IV) with a shooting method. The thresholds $r^c_{\rm stat}, r^c_{\rm osc}$ and wave numbers $\hat{k}^c_{\rm stat}, \hat{k}^c_{\rm osc}$ are reduced by the critical values $R^0_c=1707.762$ and $k^0_c=3.116\,32$ in a pure fluid.

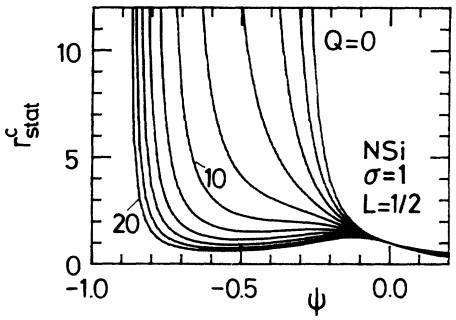

FIG. 4. Reduced stationary stability threshold of a gas mixture ($L=\frac{1}{2}$, $\sigma=1$) for NSI boundary conditions. The Dufour numbers $Q=0,2,4,\ldots,20$ increase from right to left. Increasing Q shifts the divergence r^c_{stat} to smaller ψ and strongly destabilizes the conductive state. All curves go through $\psi=0$, $r=1$ where the Dufour effect vanishes.

curves, e.g., three if Q is not too large. In Fig. 5 we have plotted the separation ratio of the intersections ψ^* against the Dufour number Q. For small Q there is only one intersection. Then, for $Q\simeq 9.3$, r^c_{stat} intersects r^c_{osc} at $\psi^*\simeq -0.12$ and touches it at $\psi^*\simeq -0.48$. For larger Q, e.g., $Q=10$ (Fig. 3), there exist three intersection points. Further increasing of Q pushes the two intersections at larger ψ values together until they coincide at $Q\simeq 11.4$ and $\psi^*\simeq -0.19$, i.e., r^c_{stat} again touches r^c_{osc}. For larger Q only the intersection at more negative ψ remains (cf. Figs. 3 and 5, $Q=20$).

Also the Hopf frequency as a function of ψ undergoes a striking development shown in Fig. 6 for $Q=0,2,4,\ldots,20$. With increasing Dufour number the curve ω_c bends down and develops a minimum ($Q=14$) at $\psi\simeq -0.5$. Then there exist two separated ranges with an oscillatory instability, e.g., for $Q=16$ one at $-0.33\le\psi\le -0.08$ and the other at $\psi<-0.63$. Increasing Q ($Q=18$) leads to a shrinking of the first range ($-0.2\le\psi\le -0.12$) and a shifting to smaller ψ of the second range ($\psi\le -0.78$) until ($Q=20$) there remains only the oscillatory range at smaller $\psi(\psi\le -0.83)$.

The topological changes due to the Dufour effect are also influenced by the size of the Lewis number. This can be seen in Fig. 7 where we show for $L=1$ and several Q the critical values at the different stability thresholds. For

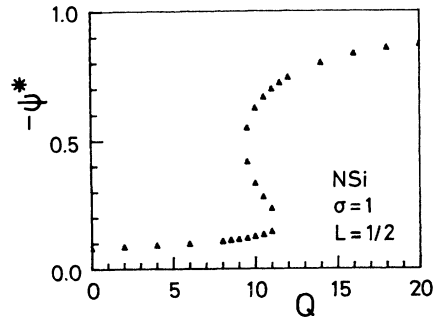

FIG. 5. Separation ratio ψ^* of the intersections between the oscillatory and stationary stability thresholds r^c_{osc} and r^c_{stat} vs the Dufour number Q for NSI boundaries. In the range $9.3\le Q\le 11.4$ the stationary stability threshold intersects the oscillatory one three times.

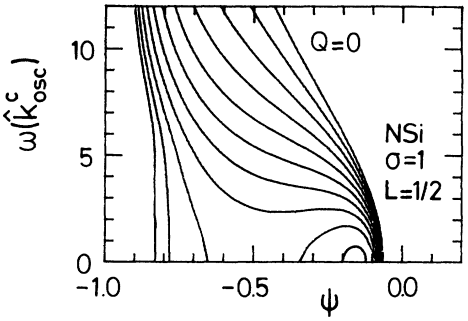

FIG. 6. Hopf frequency ω_c vs separation ratio ψ for the Dufour numbers $Q=0,2,4,\ldots,20$ (from right to left) for NSI boundaries. Increasing Q leads, via a state with two separated oscillatory ranges, to a strong shrinking of the ψ range with oscillatory instabilities.

$Q=0$ the topologies of the curves $r(\psi)$, $\hat{k}(\psi)$, and $\omega(\psi)$ are again the same as in liquid mixtures. But due to the larger Lewis number the intersection of r^c_{stat} and r^c_{osc} lies now at the much more negative $\psi^*\simeq -0.2$ than in the case of $L=\frac{1}{2}$ where $\psi^*\simeq -0.08$. Also the wave-number gap there is enlarged from $\Delta\hat{k}_c(L=\frac{1}{2})\simeq 0.2$ to $\Delta\hat{k}_c(L=1)\simeq 0.3$. Thus the Lewis number dependence of $\Delta\hat{k}_c$ is no longer linear in L as for liquid mixtures. Increasing the Dufour number to $Q=5$ shifts again the divergence of r^c_{stat} to a smaller ψ value. At the same time the oscillatory stability threshold is bent upward. Both effects together lead to a downward shift of the intersection to a smaller $\psi^*\simeq -0.7$ and larger Rayleigh number $r^*\simeq 6$. The critical wave number $\hat{k}^c_{osc}$ of the oscillatory instability now has a minimum at $\psi\simeq -0.9$ and the curve $\hat{k}^c_{stat}(\psi)$ is slightly deformed. The end point of the oscillatory threshold is shifted from $\psi^{end}_{osc}(Q=0)\simeq -0.15$ to $\psi^{end}_{osc}(Q=5)\simeq -0.23$. After increasing Q to 10 the curve $r^c_{stat}(\psi)$ has developed a minimum at $\psi\simeq -0.5$, the oscillatory threshold $r^c_{osc}(\psi)$ is bent further upward, and the intersection point is shifted to $\psi^*\simeq -0.88$, $r^*\simeq 15$. The minimum of $\hat{k}^c_{osc}(\psi)$ is more pronounced and the devel-

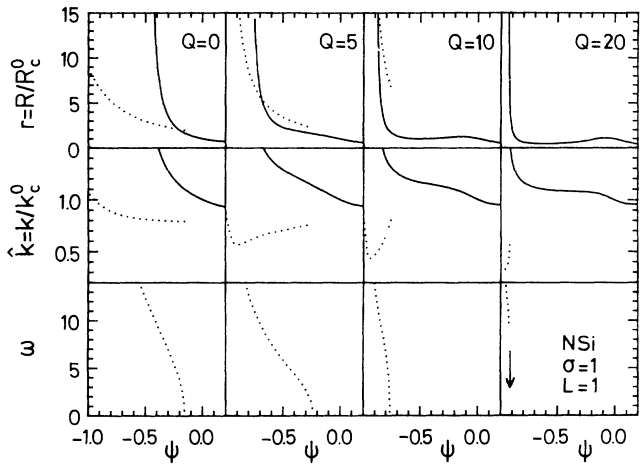

FIG. 7. Exact stability properties (solid lines, stationary; dotted lines, oscillatory) of a binary gas mixture ($L=1$, $\sigma=1$) for different Dufour numbers and NSI boundaries. For $Q=20$ the curve $\omega_c(\psi)$ drops very sharply to zero (cf. arrow) which was not resolved numerically.

opment of $\hat{k}^c_{stat}(\psi)$ as displayed in the FSI approximation can be observed. The end point of r^c_{osc} lies now at $\psi^{end}_{osc} \simeq -0.76$. Further increasing of Q leads to a general accentuation of the above-mentioned behavior, thus, e.g., for $Q=20$ the oscillatory stability threshold has moved out of the ψ-r range of Fig. 7.

The main topological differences between $L=1$ and $L=\frac{1}{2}$ are due to the different positions of the intersection points ψ^* and the different motions of the end points ψ^{end}_{osc} toward negative ψ as Q increases. For $L=1$ the end point ψ^{end}_{osc} lies to the left of the ψ range where r^c_{stat} displays a minimum-maximum combination. Thus r^c_{osc} and r^c_{stat} can intersect only once. For $L=\frac{1}{2}$ there are two separated oscillatory instability branches at large enough Q while for $L=1$ there is only one. Also this difference is due to the fact that for $L=1$ the end point ψ^{end}_{osc} moves with increasing Q so fast toward negative ψ that the Hopf frequency $\omega_c(\psi)$ cannot develop a minimum and drop to zero as for $L=\frac{1}{2}$.

B. Heating from above

Let us now briefly discuss the case when $r<0$. As already observed for thermohaline convection in binary mixtures there is also a stationary instability of the conductive state for heating from above if $\psi<0$. In Fig. 8 we present for $L=\frac{1}{2}$ the ψ dependence of this instability. Within our numerical resolution the critical stationary wave number $\hat{k}^c_{stat}$ is zero for all ψ and $Q \leq 30$, for which we have performed a numerical NSI analysis. The *critical* Rayleigh number r^c_{stat} (dashed line in Fig. 8) is the same for all $Q \leq 30$. Thus the Dufour effect has no influence on the zero wave-number instability for $r<0$. But this is no longer true if the geometry selects a finite $\hat{k}$ value at the onset of convection. Then increasing the Dufour number shifts the stability threshold to more negative ψ and thus changes the stability of the conductive state. In Fig. 8 we show with solid lines as a representative example $r_{stat}(\hat{k}=1)$ for $Q=0,10,20,30$. Note that all curves merge at $\psi=-1$. Thus we have for $\psi>-1$ a stabilization of the conductive state by the Dufour effect and for $\psi<-1$ a destabilization. At $\psi=-1$ the driving from the temperature field in (3.11a) drops out and the driving force is only the ζ field. These features are not reproduced properly by our FSI approximation since in the numerator of (3.2) the Dufour contribution is weighted by $(1-8/\pi^2)$. This factor arises from the projection of the approximated modes.

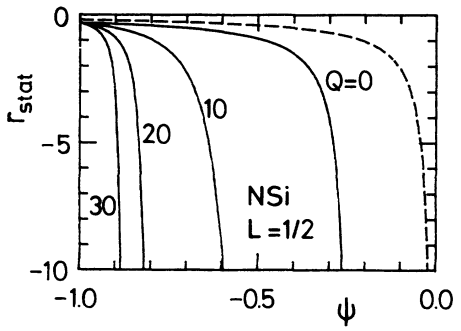

FIG. 8. Reduced stability threshold for the onset of stationary convection in a binary gas ($L=\frac{1}{2}$, $\sigma=1$) layer heated from above. The boundary conditions are NSI. The influence of the Dufour effect on the stability at a finite k is illustrated for $k=k_c^0=3.116\,32$ and several Q values (solid lines). All curves intersect at $\psi=-1$. The critical quantities $k^c_{stat}=0$ and r^c_{stat} are independent of Q. The dashed line shows $r_{stat}(k=10^{-3})$.

V. CONCLUSIONS AND PERSPECTIVE

We have investigated the influence of the Dufour effect, i.e., the effect that concentration fluxes generate temperature fluctuations on the stability behavior of the conductive state of binary fluid mixtures in the Rayleigh-Bénard setup. To that end we have applied three different boundary conditions to the convective perturbations of the conductive state: idealized free-slip permeable boundary conditions, more realistic free-slip impermeable boundary conditions, and realistic no-slip impermeable ones. An exact (approximate) analytical approach was presented for the FSP (FSI) case and then compared with the exact numerical solutions for the NSI case which can be taken as quantitative predictions relevant for experiments.

Our results are as follows. (1) In *liquid* mixtures where $L \simeq 10^{-2}$ and $Q \simeq 10^{-1}$ the Dufour effect has no significant influence on the stability thresholds. They differ by less than 1%. (2) In *gas* mixtures where L is of order unity and Q of the order 10 the stability thresholds differ substantially in comparison to the case without Dufour effect, $Q=0$. We have estimated the size of the Dufour numbers in gases with an ideal-gas approximation. It shows that Q can be quite large in dilute mixtures having a minimum if the concentrations of the two components and the particle masses are similar. Calculations [40] for C_2H_6-CO_2 support our estimates. An experimental determination of the Dufour number would be helpful. (3) The changes in the NSI stability properties caused by the Dufour effect are in detail: (i) extension of the existence range of the stationary instability toward more negative ψ and mainly a destabilization of the conductive state against stationary perturbations; (ii) shift of the intersection point ψ^* and of the end point ψ^{end}_{osc} of the oscillatory threshold to more negative ψ; (iii) diminishing of the range of the oscillatory instability and stabilization of the conductive state against oscillatory perturbations; (iv) existence of separate oscillatory threshold curves for appropriate L-Q parameters. (4) The analytical FSP results show largely the same behavior of the stability thresholds, but no information on the ψ and Q dependence of the critical wave numbers. This information can be obtained from our FSI calculations in an approximate manner as well as the other stability properties. Detailed discussions with varying Q for two representative Lewis numbers ($L=\frac{1}{2}$, $L=1$) were presented as quantitative predictions for experiments.

Let us now discuss some experimental implications of our analysis. The most striking implication of experimental relevance seems to be the drastic shift and the diminishing of the oscillatory range to more negative ψ.

Thus, e.g., in gas mixtures with $L=1$, $\sigma=1$, $Q>5$ only a stationary stability threshold is observable in experiments that are restricted to separation ratios $\psi \gtrsim -0.2$. But the knowledge about the accessible ψ values in various gas mixtures seems to be limited. A possible way to reach more negative ψ might be working near a critical point where the ratio of the expansion coefficients β/α takes on very large values. Since the Dufour number is proportional to α^2/β^2, this, however, implies a suppression of the influence of the Dufour effect. Another point which affects quantitative comparisons of our predictions with experiments is that the Soret-induced concentration gradient of the conductive state is in gas mixtures bigger than in liquids [32]. An upper limit [32] for the validity of the Oberbeck-Boussinesq approximation implies that too small a height of the convection cell can lead to a breakdown of that approximation used in this work

ACKNOWLEDGMENT

This work was supported by Deutsche Forschungsgemeinschaft.

APPENDIX: IDEAL BINARY GAS MIXTURES

Here we collect known formulas for the solutal expansion coefficient β and the derivative of the chemical potential with respect to the concentration $(\partial\mu/\partial C)_{T,p}$, both entering into the Dufour number Q for ideal-gas mixtures which will be a reasonable approximation for real ones. We furthermore estimate the influence of compressibility on the buoyancy force. Throughout this appendix we use unreduced quantities with their proper dimensions.

1. Dufour number

The mass densities of the single components of the binary mixtures ρ_1 and ρ_2 are

$$\rho_1 = C\rho \quad \text{and} \quad \rho_2 = (1-C)\rho \ , \tag{A1}$$

where ρ is the total mass density and C the concentration of the lighter component. The corresponding particle densities are

$$n_1 = \frac{\rho_1}{m_1} \quad \text{and} \quad n_2 = \frac{\rho_2}{m_2} \ , \tag{A2}$$

where m_1 and m_2 are the particle masses of components 1 and 2, respectively. Thus the total particle density is

$$n = n_1 + n_2 = \rho \left[\frac{C}{m_1} + \frac{1-C}{m_2} \right] \tag{A3}$$

and the pressure $p = nk_B T$ is given by

$$\rho = \frac{p}{k_B T} \frac{m_1 m_2}{(1-C)m_1 + Cm_2} \tag{A4}$$

with k_B denoting Boltzmann's constant. From Eq. (A4) one obtains the solutal expansion coefficient.

$$\beta = -\frac{1}{\rho} \left[\frac{\partial \rho}{\partial C} \right]_{T,p} = \frac{m_2 - m_1}{(1-C)m_1 + Cm_2} \ . \tag{A5}$$

Thus the smaller the difference between the masses of the molecules of the different components the smaller is β and the higher the Dufour number $Q \sim 1/\beta^2$. Since C is the concentration of the lighter component in the mixture, i.e., $m_1 < m_2$, the solutal expansion coefficient of the ideal-gas mixture is positive, $\beta > 0$. Moreover β of the ideal-gas mixture depends on neither the temperature nor the pressure. For very dilute mixtures $C \ll 1$ one finds $\beta \simeq m_2/m_1 - 1$.

The chemical potential μ in binary mixtures is defined by [35]

$$\mu = \mu_1/m_1 - \mu_2/m_2 \ , \tag{A6}$$

where μ_1 and μ_2 are the chemical potentials of the single components. In an ideal-gas mixture [35]

$$\mu_i = f_i(p,T) + k_B T \ln \frac{n_i}{n_1 + n_2} \tag{A7}$$

with $i=1$ or 2 and f_i independent of the concentration. Using (A2) and (A7) one obtains

$$\left[\frac{\partial \mu}{\partial C} \right]_{T,p} = \frac{k_B T}{(1-C)m_1 + Cm_2} \left[\frac{1}{C} + \frac{1}{1-C} \right] \ . \tag{A8}$$

Thus $(\partial\mu/\partial C)_{T,p}$ grows linearly with temperature and does not depend on the pressure. Moreover for very small and very high concentrations, i.e., $C \to 0$ or $C \to 1$, $(\partial\mu/\partial C)_{T,p}$ diverges. Since the Dufour number Q is proportional to $(\partial\mu/\partial C)_{T,p}$ large Dufour numbers can be realized in very dilute gas mixtures.

In Fig. 9 we show the ideal-gas approximation for a representative mixture C_2H_6-CO_2 (the molar mass of C_2H_6 is 30 g/mol and of CO_2 44 g/mol) at a temperature of about 300 K. The dashed line represents 20β according to (A5). Thus β varies nearly linearly between about

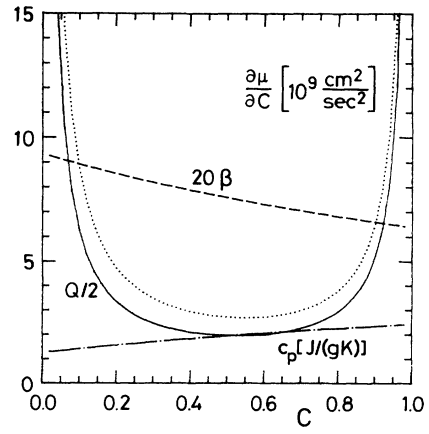

FIG. 9. Thermodynamic properties of gas mixtures. The solutal expansion coefficient β and $(\partial\mu/\partial C)_{T,P}$ is evaluated for ideal-gas mixtures while the specific heat is extrapolated from Ref. [41]. The resulting Dufour number should be reasonably realistic for C_2H_6-CO_2 mixtures at room temperature.

0.475 for small C down to 0.325 for large C. The dotted line shows $(\partial\mu/\partial C)_{T,p}$, given in units of 10^9 cm^2/sec^2. It diverges for $C\to 0$ and $C\to 1$ and has its minimum value of about 2.5 for $C\simeq\frac{1}{2}$. The specific heat c_p [given in units of J/(g K)] is extrapolated from tables and shows for growing concentrations a slight increase with C from about 1 J/(g K) to 2.5 J/(g K). The thermal expansion coefficient α of the ideal-gas mixture is 1/(273 K). The solid line in Fig. 9 represents half the Dufour number (2.8) calculated with (A5) and (A8) and the thermal expansion coefficient $\alpha=1/(273\text{ K})$ of an ideal-gas mixture. It shows a similar behavior as $(\partial\mu/\partial C)_{T,p}$. It diverges for $C\to 0$ and $C\to 1$ and its minimal value $Q=4$ at about $C=0.55$. The order of magnitude of Q coincides with an estimate given for typical real-gas mixtures in Ref. [31]. Note finally that the mean pressure does not enter into the calculation of Q within the ideal-gas approximation.

2. Influence of compressibility on buoyancy

The compressibility coefficient χ, following from (A4), is given by

$$\chi=\frac{1}{\rho}\left[\frac{\partial\rho}{\partial p}\right]_{T,C}=\frac{1}{p}\ . \tag{A9}$$

Thus the smaller the mean pressure the larger the compressibility coefficient. Pressure gradients in the density entering the buoyancy term

$$\rho=\rho_0(1-\alpha\Delta T-\beta\Delta C+\chi\Delta p) \tag{A10}$$

lead to significant contributions whenever $|\chi\Delta p|$ is comparable with $|\alpha\Delta T|$ and $|\beta\Delta C|$. The maximum pressure gradient is given by $\Delta p=\rho g d$. Assuming typical values of $\kappa=\nu=10^{-1}$ cm^2/sec, $d=1$ cm and $\Delta T\simeq 5$ K corresponding to a Rayleigh number $R=1700$ one finds $|\alpha\Delta T|\sim 10^{-3}$, $|\beta\Delta C|\sim\psi\times 10^{-3}$, and $|\chi\Delta p|\sim 10^{-6}$. Thus compressibility in the buoyancy term is of the order of the concentration contribution in Eq. (A10) if $|\psi|<10^{-3}$. But in that case the temperature contribution dominates the density differences and both other contributions are negligible.

[1] For a review see J. K. Platten and J. C. Legros, *Convection in Fluids* (Springer, Berlin, 1984) and references cited therein. References to work published thereafter may be found in Refs. [2–13] ([14–34]) describing some recent experimental (theoretical) work on convection in binary liquid mixtures.

[2] O. Lhost and J. K. Platten, Phys. Rev. A **40**, 6415 (1989).

[3] V. Steinberg, J. Fineberg, E. Moses, and I. Rehberg, Physica D **37**, 359 (1989); E. Moses and V. Steinberg, Phys. Rev. A **43**, 707 (1991).

[4] J. J. Niemela, G. Ahlers, and D. S. Cannell, Phys. Rev. Lett. **64**, 1365 (1990).

[5] D. Bensimon, P. Kolodner, C. M. Surko, H. Williams, and V. Croquette, J. Fluid Mech. **217**, 441 (1990).

[6] P. Bigazzi, S. Ciliberto, and V. Croquette, J. Phys. (Paris) **51**, 611 (1990).

[7] P. Kolodner, Phys. Rev. Lett. **66**, 1165 (1991).

[8] C. M. Surko, D. R. Ohlsen, S. Y. Yamamoto, and P. Kolodner, Phys. Rev. A **43**, 7101 (1991).

[9] K. D. Eaton, D. R. Ohlsen, S. Y. Yamamoto, C. M. Surko, W. Barten, M. Lücke, M. Kamps, and P. Kolodner, Phys. Rev. A **43**, 7105 (1991).

[10] G. Zimmermann and U. Müller (unpublished).

[11] R. E. Ecke, H. Haucke, Y. Maeno, and J. C. Wheatley, Phys. Rev. A **33**, 1870 (1986).

[12] M. Gao and R. P. Behringer, Phys. Rev. A **35**, 3993 (1987).

[13] T. S. Sullivan and G. Ahlers, Phys. Rev. A **38**, 3143 (1988).

[14] D. Gutkowicz-Krusin, M. A. Collins, and I. Ross, Phys. Fluids **22**, 1443; **22**, 1451 (1979).

[15] G. W. T. Lee, P. Lucas, and A. Tyler, J. Fluid Mech. **135**, 235 (1983).

[16] P. L. G. Ybarra and M. G. Velarde, Geophys. Astrophys. Fluid Dyn. **13**, 83 (1979).

[17] G. Vanderborck and J. K. Platten, Rev. Gen. Therm. **190**, 693 (1977).

[18] H. R. Brand, P. C. Hohenberg, and V. Steinberg, Phys. Rev. A **30**, 2548 (1984).

[19] E. Knobloch, Phys. Rev. A **34**, 1538 (1986).

[20] M. C. Cross, Phys. Rev. Lett. **57**, 2935 (1986); Phys. Rev. A **38**, 3593 (1988).

[21] S. J. Linz and M. Lücke, Phys. Rev. A **35**, 3997 (1987); in *Propagation in Systems far from Equilibrium,* Springer Series in Synergetics Vol. 41 (Springer, Berlin, 1988), p. 292.

[22] S. J. Linz and M. Lücke, Phys. Rev. A **36**, 3505 (1987).

[23] E. Knobloch and D. R. Moore, Phys. Rev. A **37**, 860 (1988).

[24] M. C. Cross and K. Kim, Phys. Rev. A **37**, 3909 (1988); **38**, 529 (1988).

[25] S. J. Linz, M. Lücke, H. W. Müller, and J. Niederländer, Phys. Rev. A **38**, 5727 (1988).

[26] W. Schöpf and W. Zimmermann, Europhys. Lett. **8**, 41 (1989).

[27] D. Bensimon, A. Pumir, and B. Shraiman, J. Phys. (Paris) **50**, 3089 (1989).

[28] W. Barten, M. Lücke, W. Hort, and M. Kamps, Phys. Rev. Lett. **63**, 376 (1989); W. Barten, M. Lücke, and M. Kamps *ibid.* **66**, 2621 (1991).

[29] M. Bestehorn, R. Friedrich, and H. Haken, Z. Phys. B **75**, 265 (1989).

[30] H. Yahata, Progr. Theoret. Phys. Suppl. **99**, 493 (1989).

[31] S. J. Linz, Phys. Rev. A **40**, 7175 (1989); **45**, 1262 (1992).

[32] W. Hort, S. J. Linz, and M. Lücke, in *Nonlinear Evolution of Spatio-temporal Structures in Dissipative Continuous Systems,* Vol. 225 of *NATO Advanced-Study Institute, Series B: Physics,* edited by F. H. Busse, and L. Kramer (Plenum, New York, 1990), p. 149.

[33] W. Hort, Diplomarbeit, Universität Saarbrücken, 1990.

[34] O. Lhost, S. J. Linz, and H. W. Müller, J. Phys. (Paris) II **1**, 279 (1991).

[35] L. D. Landau and E. M. Lifshitz, *Fluid Mechanics* (Pergamon, New York, 1959).

[36] G. Z. Gershuni and E. M. Zhukhovitskii, *Convective Sta-*

bility of Incompressible Fluids (Keter, Jerusalem, 1976).
[37] N. D. Stein, Phys. Rev. A **43**, 768 (1991).
[38] S. R. deGroot and P. Mazur, *Non-equilibrium Thermodynamics* (North-Holland, Amsterdam, 1962).
[39] M. G. Velarde, in *Chaos and Order in Nature,* Springer Series in Synergetics Vol. 11 (Springer, Berlin, 1982), p. 132.
[40] J. deBruijn (private communication); E. Bodenschatz and G. Ahlers (private communication).
[41] *American Institute of Physics Handbook,* edited by D. E. Gray (McGraw-Hill, New York, 1972).